

## Melting of size-selected aluminum nanoclusters with 84–128 atoms

Anne K. Starace, Baopeng Cao, Oscar H. Judd, Indrani Bhattacharyya, and Martin F. Jarrold<sup>a)</sup>

*Department of Chemistry, Indiana University, 800 East Kirkwood Ave., Bloomington, Indiana 47405, USA*

(Received 18 October 2009; accepted 13 December 2009; published online 15 January 2010)

Heat capacities have been measured as a function of temperature for isolated aluminum nanoclusters with 84–128 atoms. Most clusters show a single sharp peak in the heat capacity which is attributed to a melting transition. However, there are several size regimes where additional features are observed; for clusters with 84–89 atoms the peak in the heat capacity is either broad or bimodal. For  $\text{Al}_{115}^+$ ,  $\text{Al}_{116}^+$ , and  $\text{Al}_{117}^+$  there are two well-defined peaks, and for  $\text{Al}_{126}^+$ ,  $\text{Al}_{127}^+$ , and  $\text{Al}_{128}^+$  there is a dip in the heat capacity at lower temperature than the peak. The broad or bimodal peaks for clusters with 84–89 atoms are not significantly changed by annealing to 823 K (above the melting temperature), but the dips for  $\text{Al}_{126}^+$ ,  $\text{Al}_{127}^+$ , and  $\text{Al}_{128}^+$  disappear when these clusters are annealed to 523 K (above the temperature of the dip but below the melting temperature). Both the melting temperatures and the latent heats change fairly smoothly with the cluster size in the size regime examined here. There are steps in the melting temperatures for clusters with around 100 and 117 atoms. The step at  $\text{Al}_{100}^+$  is correlated with a substantial peak in the latent heats but the step at  $\text{Al}_{117}^+$  correlates with a minimum. Since the latent heats are correlated with the cluster cohesive energies, the substantial peak in the latent heats at  $\text{Al}_{100}^+$  indicates this cluster is particularly strongly bound. © 2010 American Institute of Physics. [doi:10.1063/1.3285836]

### I. INTRODUCTION

Metal nanoclusters have attracted attention because they have important applications in catalysis, optics, medicine, and nanoelectronic devices.<sup>1</sup> Clusters with less than a few hundred atoms show size-specific features in their structures,<sup>2–5</sup> cohesive energies,<sup>6–8</sup> and thermodynamic properties.<sup>9–11</sup> For example, the structures of some sodium clusters can change from a disordered morphology to a geometry with global order with the addition of one or two atoms.<sup>12</sup> Adding an atom to some gallium clusters changes the melting transition from first-order to a second.<sup>13</sup> These strong size-dependent characteristics make the study of nanoclusters with up to a few hundred atoms both interesting and challenging.

In this paper we address the size dependence of the melting transition. There has been interest in how size affects the melting point of a metal particle since the important work of Pawlow a century ago.<sup>14</sup> He predicted that the melting points of small particles are depressed due to the increase in the surface-to-volume ratio, the depression scaling as  $1/r$ . For particles with less than a few hundred atoms the melting temperature and latent heat can become strongly size dependent.<sup>9,15,16</sup> Changing the cluster size by even a single atom can cause a substantial difference in the melting behavior.

Considerable effort has been invested in trying to understand the size dependent fluctuations in the melting temperatures and latent heats that occur for clusters with less than a few hundred atoms.<sup>17–27</sup> It is now understood that the latent

heats are correlated with the cohesive energies of the solid clusters.<sup>28</sup> Liquid clusters have cohesive energies that are not strongly size dependent, so fluctuations in the latent heats lead to, or result from (depending on your point of view), fluctuations in the cohesive energies of the solid clusters. The wide variations in the melting temperatures that occur with cluster size have been difficult to explain. Sodium and aluminum clusters have been the most widely studied. For sodium clusters it appears that variations in the melting temperatures are correlated with geometric shell closings for icosahedral geometries.<sup>20–22,26</sup> For the aluminum clusters studied so far, both geometry and the electronic structure are important.<sup>28,29</sup> There are substantial maxima in the melting temperatures around the spherical electronic shell closings with 138 ( $\text{Al}_{46}$ ) and 198 ( $\text{Al}_{66}$ ) valence electrons. There are no substantial maxima in the latent heats for these clusters, so it is thought that the maxima in the melting temperature result mainly from entropic effects. According to calculations,<sup>28,29</sup> the clusters around the shell closings with 138 and 198 valence electrons adopt near-spherical geometries that are disordered. The disordered geometries cause the entropy change on melting to be diminished which leads to an elevated melting temperature (because  $T_m = \Delta H_m / \Delta S_m$ , where  $T_m$  is the melting temperature, and  $\Delta H_m$  and  $\Delta S_m$  are the enthalpy and entropy changes).

We previously reported heat capacity measurements for aluminum clusters with 16–83 atoms.<sup>10,16,30</sup> In this paper we extend these measurements to larger cluster sizes. Specifically we report heat capacity measurements as a function of temperature for size-selected  $\text{Al}_n^+$  with  $n=84–128$ . Features in the heat capacities (peaks and dips) are used to identify structural transitions and melting transitions. Our results for

<sup>a)</sup> Author to whom correspondence should be addressed. Electronic mail: mfj@indiana.edu.

$\text{Al}_{115}^+$ ,  $\text{Al}_{116}^+$ , and  $\text{Al}_{117}^+$  have been discussed in detail elsewhere;<sup>31</sup> these clusters have two clearly resolved peaks in their heat capacities. The low temperature peak has been assigned to a structural transition involving a superheated solid, and the high temperature peak is attributed to a melting transition.

Heat capacity measurements have been by far the most widely used approach to investigate the melting transitions of metal nanoclusters. The method hinges on measuring the change in internal energy resulting from a temperature change. In the pioneering studies of Haberland and co-workers the change in the internal energy is determined from the change in the number of evaporation steps that occur following multiphoton excitation.<sup>15</sup> The photon energy must be large compared to the dissociation energy of the cluster for this approach. It has been used to study the melting of sodium clusters.<sup>9,15,20</sup> In the experiments described here we use multicollision induced dissociation to determine the heat capacity.<sup>32</sup> In this approach, the amount of energy that must be added to induce the clusters to dissociate is determined. The cluster's initial temperature is raised, and then the energy that must be added to cause dissociation is remeasured. The change in the amount of energy that must be added divided by the change in temperature gives the heat capacity. This method has been applied to a wide range of pure metal clusters (gallium,<sup>32,33</sup> tin,<sup>34</sup> and aluminum<sup>16,27,30</sup>) and alloy clusters.<sup>35,36</sup> Recently Chirot *et al.*<sup>37</sup> described another method of determining heat capacities for size selected nanoclusters which is based on sticking additional atoms onto the cluster. This method has also been used to study sodium clusters.

## II. EXPERIMENTAL METHODS

As noted above, our heat capacity measurements hinge on measuring the amount of energy needed to dissociate the clusters as a function of their initial temperature. To perform this measurement, a beam of size-selected cluster ions is focused into a collision cell containing 1.0 torr of helium gas. As the clusters enter the collision cell, they undergo numerous collisions with helium, each one converting a small fraction of the cluster ion's translational energy into internal energy. If the cluster ions' initial translational energy is large enough, they are heated to the point where dissociation occurs. The fragment ions and undissociated clusters are directed across the collision cell by a weak electric field. Some of them exit through a small aperture and they are then focused into a quadrupole mass spectrometer. The fraction that dissociates is determined from the mass spectrum. Similar measurements are performed with around six values of the cluster ion's initial translational energy (the translational energy with which the cluster ions enter the collision cell), and then a linear regression is used to determine the translational energy required for 50% of the cluster ions to dissociate (TE50%D). The cluster temperature is then changed (see below) and TE50%D is remeasured. The derivative of TE50%D with respect to the temperature is proportional to the heat capacity. The proportionality constant is the fraction

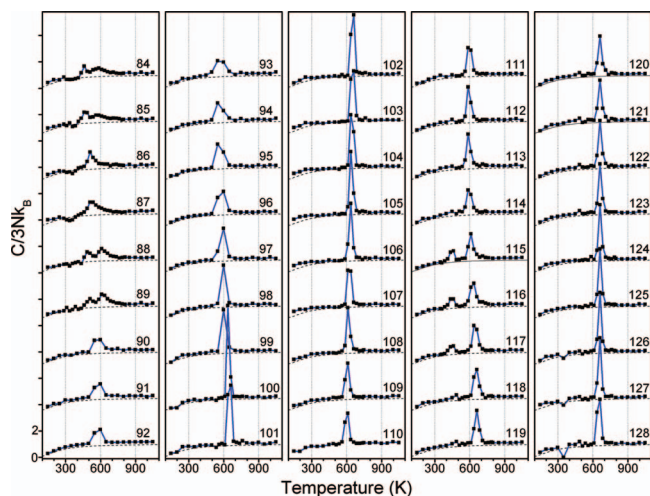


FIG. 1. Heat capacities measured as a function of temperatures for clusters with 84 to 128 atoms. The heat capacities are in units of  $3Nk_B$ , where  $3N=3n-6+3/2$ , and  $k_B$  is the Boltzmann constant. The filled black squares are the measured values. The solid blue lines are guides. The dashed black lines are heat capacities calculated with a modified Debye model (Ref. 41). Both the size and position of the heat capacity peak change with the cluster size.

of the ion's translational energy that is converted into internal energy during a collision. This quantity is deduced from an impulsive collision model.<sup>38</sup>

The aluminum cluster ions are generated by laser vaporization of a liquid metal target<sup>39</sup> in a continuous flow of helium buffer gas. After formation, the clusters are carried by the helium buffer gas flow (around 350 standard cubic centimeters per second) into a temperature variable extension where their temperature is set by equilibration with the walls of the extension through collisions with the buffer gas. At the end of the extension, the clusters exit through a small aperture and they are then focused into a quadrupole mass spectrometer set to transmit a specific cluster size. At the end of the quadrupole, the size selected clusters are focused into the collision cell.

In some of the experiments the clusters were annealed before having their temperature set for the heat capacity measurements. For these studies an annealing section is inserted between the source region and the temperature variable extension. The annealing temperature can be independently varied from room temperature to 1200 K. A detailed description of the annealing section has been published elsewhere.<sup>40</sup>

## III. EXPERIMENTAL RESULTS FOR UNANNEALED CLUSTERS

Figure 1 shows the heat capacities measured as a function of temperature for  $\text{Al}_n^+$  with 84–128 atoms. The black squares are the measured values. The solid blue lines are guides. The dashed lines are the heat capacities calculated from a modified Debye model.<sup>41</sup> The heat capacities are plotted in the units of the classical value,  $3Nk_B$ , where  $3N=(3n-6+3/2)$ ,  $k_B$  is the Boltzmann constant, and  $n$  is the number of atoms in the cluster. Initially we measured the heat capacities from 148 to 1048 K in 50 K increments ( $\Delta T=50$  K) to locate the main features. For clusters with

84–89 and 100–128 atoms we then re-measured the heat capacities around the main features with  $\Delta T=25$  K. In Fig. 1 we show the  $\Delta T=25$  K data where it is available, and the  $\Delta T=50$  K data where it is not. The  $\Delta T=25$  K data offers the benefit of higher resolution, but the measurements are noisier (particularly for  $\text{Al}_{84}$ – $\text{Al}_{89}$ ). In both cases, the results shown in the figure are an average of multiple measurements. Enough measurements were performed to ensure that the average values given in the figure are reliable.

It is evident from Fig. 1 that clusters with 84, 85, 88, and 89 atoms have bimodal peaks with components that are resolved but not fully separated. Clusters with 86 and 87 atoms have a broad peak.  $\text{Al}_{115}^+$ ,  $\text{Al}_{116}^+$ , and  $\text{Al}_{117}^+$  have two well-separated peaks.  $\text{Al}_{126}^+$ ,  $\text{Al}_{127}^+$ , and  $\text{Al}_{128}^+$  have a dip at around 350 K followed by a peak at around 650 K. The rest of the clusters in the 84–128 atom size range have a single peak in the heat capacity which we attribute to a melting transition. The results for  $\text{Al}_{115}^+$ ,  $\text{Al}_{116}^+$ , and  $\text{Al}_{117}^+$  have been discussed elsewhere.<sup>31</sup> Annealing studies were performed for these clusters and we assigned the lower temperature peak to a solid-to-solid transition and the higher temperature peak to a melting transition.

We determine the transition temperatures and latent heats by fitting the measured heat capacities with a two-state or three-state model, depending on the number of features present. These models have been described previously.<sup>10,31,40,42</sup> We assume that melting occurs in the dynamic phase coexistence limit, where for the two-state system the transition is between fully solid and fully liquid clusters (i.e., there are no partially melted intermediates). This behavior was first observed in simulations.<sup>43–50</sup> There is now experimental evidence that dynamic phase coexistence occurs for aluminum clusters in the size range examined here.<sup>51</sup> In this limit, the liquid and solid clusters are in equilibrium with an equilibrium constant given by

$$K(T) = \frac{f_L(T)}{f_S(T)} \exp \left[ -\frac{\Delta H_m}{R} \left( \frac{1}{T} - \frac{1}{T_m} \right) \right]. \quad (1)$$

In this equation,  $f_L(T)$  and  $f_S(T)$  are the fractions of liquid and solid clusters present at temperature  $T$ ,  $\Delta H_m$  is the latent heat,  $T_m$  is the melting temperature (where the amounts of liquid and solid present are equal), and  $R$  is the gas constant. The contribution of the latent heat to the heat capacity is

$$C(T) = \frac{dE_{\text{int}}}{dT} = \frac{\Delta(f_L(T)\Delta H_m)}{\Delta T}. \quad (2)$$

We add this to the heat capacity due to the internal energy of the solid and liquid clusters. For both, we use the heat capacity derived from the modified Debye model<sup>41</sup> multiplied by a scale factor. The simulation is fit to the measured heat capacities using a least-squares procedure with four adjustable parameters:  $\Delta H_m$ ,  $T_m$ ,  $S_S$ , and  $S_L$ , where  $S_S$  and  $S_L$  are scale factors. We found that clusters with heat capacities dominated by a single sharp peak (90–114 and 118–125 atoms) are well fit by the two-state model. Figure 2 shows some representative examples. In this figure, the filled black squares are the measured heat capacities, and the open blue circles are the fit to the measured points using the same value

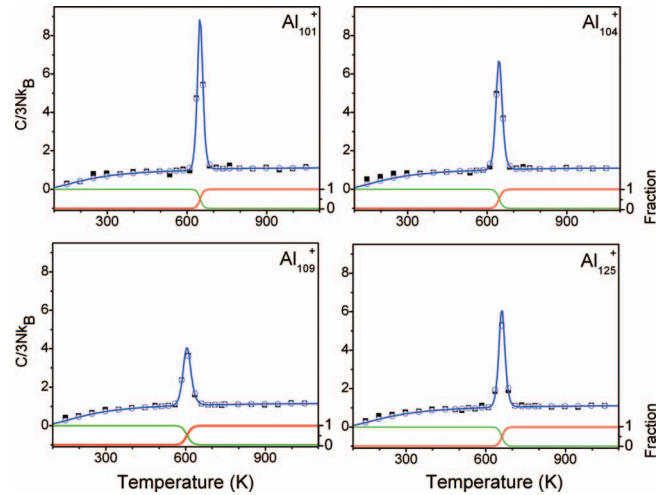


FIG. 2. Examples of fits to the measured heat capacities using the two-state model (see text). Results are shown for  $\text{Al}_{101}^+$ ,  $\text{Al}_{104}^+$ ,  $\text{Al}_{109}^+$ , and  $\text{Al}_{125}^+$ . The heat capacities are in units of  $3Nk_B$ , where  $3N=3n-6+3/2$ , and  $k_B$  is the Boltzmann constant. The filled black squares represent the measured heat capacities and the open blue circles are the fits to the experimental points using the same  $\Delta T$  as used in the experiments (25 K or 50 K). The solid blue lines are calculated with  $\Delta T=5$  K. The green and red lines at the bottom of each plot are the fractions of the solid and liquid clusters, respectively.

of  $\Delta T$  as used in the experiments (25 K or 50 K). The solid blue lines are heat capacities calculated with  $\Delta T=5$  K which is much smaller than used in the experiments. The line goes through the points, indicating that the value of  $\Delta T$  used in the measurements is small enough that the peaks are not significantly broadened. The red and green lines in the figure show the fractions of liquid and solid clusters obtained from the fit, as a function of temperature.

For most of the clusters there are at least three points across the peak in the heat capacity (see results for  $\text{Al}_{109}^+$  and  $\text{Al}_{125}^+$  in Fig. 2). However, for some clusters there are only two measurements because the peaks are very narrow (see results for  $\text{Al}_{101}^+$  and  $\text{Al}_{104}^+$  in Fig. 2). The number of measurements across the heat capacity peak has an effect on the accuracy of the melting temperature and latent heat determined from the fit. This was investigated by fitting results obtained for the same cluster with  $\Delta T=50$  and 25 K. Most clusters have two measurements across the peak for  $\Delta T=50$  K and three measurements with  $\Delta T=25$  K. For these cases, the melting temperatures obtained from the fits of the data with  $\Delta T=25$  K usually differ from the values obtained with  $\Delta T=50$  K by less than 3 K. The latent heats usually differ by less than 5%. Thus reasonably reliable values for the melting temperatures and latent heats can be obtained from just two measurements across the peak, but three or more measurements (as employed here in most cases) are preferable for more accurate values.

For clusters with 126, 127, and 128 atoms, there is a dip in the heat capacity at a significantly lower temperature than the peak. Since the dips are well separated from the peaks, we can fit the peaks independently with the two-state model, neglecting the dips. Figure 3 shows heat capacities (black solid squares) recorded for  $\text{Al}_{128}^+$  in the region of the dip. In

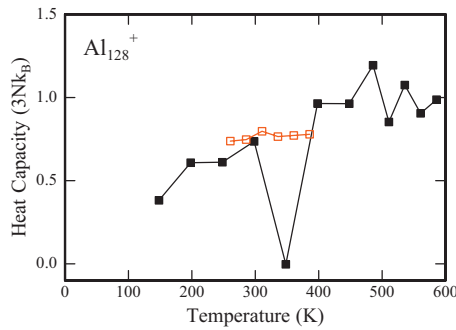


FIG. 3. Heat capacities measured for  $\text{Al}_{128}^+$  around the dip at 300–400 K. The heat capacities are in units of  $3Nk_B$ , where  $3N=3n-6+3/2$ , and  $k_B$  is the Boltzmann constant. The filled black squares are the measured heat capacities for unannealed clusters. The open red squares show heat capacities measured for clusters that were annealed to 523 K.

this case the measured heat capacity drops to around zero at 350 K. The red, unfilled squares are data for annealed clusters which are discussed later.

For the clusters that have bimodal peaks (84, 85, 88, and 89) or a broad peak (86, and 87), the two-state model does not work, and a three-state model involving an intermediate was used to fit the peaks<sup>10,31,40,42</sup>

$$S \rightleftharpoons I \rightleftharpoons L. \quad (3)$$

The intermediate may be a partially melted cluster where some part of the cluster (for example the surface) melts before the rest, or it could be due to another solid state structure which becomes accessible (thermodynamically and kinetically) as the cluster is heated. We already discussed the results for  $\text{Al}_{115}^+$ ,  $\text{Al}_{116}^+$ , and  $\text{Al}_{117}^+$  where there are two well-separated peaks in the heat capacity (see Fig. 1). In this case, annealing studies suggest that the intermediate is another solid state.<sup>31</sup> In the dynamic coexistence limit, both transitions in the three-state model are described by equilibrium constants:

$$K_M(T) = \exp\left[\frac{-\Delta H_M}{R}\left(\frac{1}{T} - \frac{1}{T_M}\right)\right], \quad (4)$$

$$K_{SS}(T) = \exp\left[\frac{-\Delta H_{SS}}{R}\left(\frac{1}{T} - \frac{1}{T_{SS}}\right)\right], \quad (5)$$

where  $K_1$ ,  $\Delta H_1$ , and  $T_1$  are the equilibrium constant, enthalpy change (latent heat), and transition temperature for the first transition and  $K_2$ ,  $\Delta H_2$ , and  $T_2$  are the same for the second. The contributions of the enthalpy changes for the two transitions to the internal energy and to the heat capacity are

$$E_{IE}(T) = (f_I(T) + f_L(T))\Delta H_1 + f_L(T)\Delta H_2, \quad (6)$$

$$C(T) = \frac{dE_{IE}(T)}{dT} = \frac{\Delta[(f_I(T) + f_L(T))\Delta H_1 + f_L(T)\Delta H_2]}{\Delta T}, \quad (7)$$

where  $f_S(T)$ ,  $f_I(T)$ , and  $f_L(T)$  are the fractions of the solid, the intermediate, and the liquid present at temperature  $T$ . We add this to the component of the heat capacity due to the internal energy of the solid, intermediate, and liquid clusters which we obtain from the modified Debye model<sup>41</sup> multi-

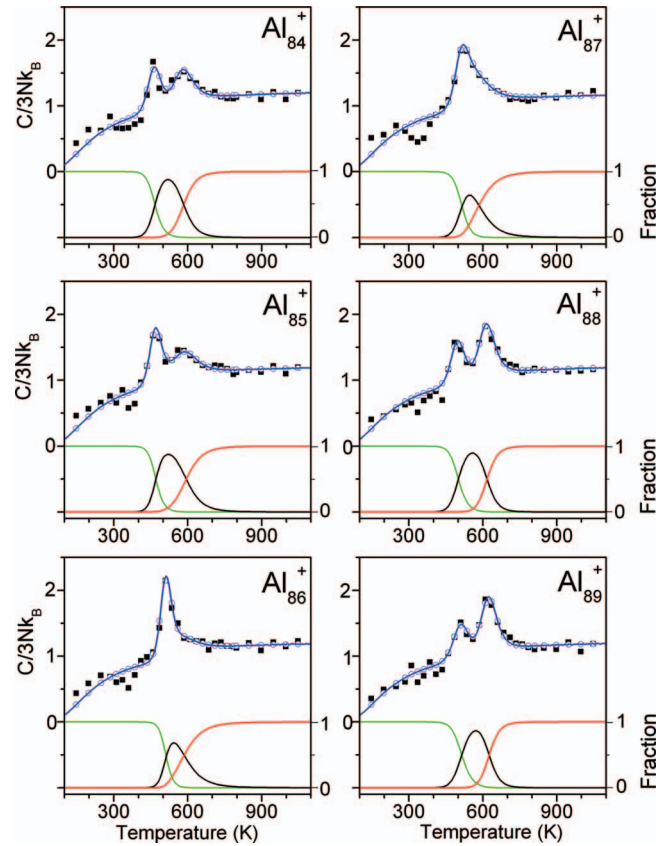


FIG. 4. Results of the fits using the three-state model (see text) to the measured heat capacities for clusters with 84–89 atoms. The heat capacities are in units of  $3Nk_B$ , where  $3N=3n-6+3/2$ , and  $k_B$  is the Boltzmann constant. The filled black squares are the measured heat capacities and the open blue circles are the fit to the measured points with the same  $\Delta T$  as used in the experiments (25 K or 50 K). The solid blue line is the calculated heat capacity with  $\Delta T=5$  K. The green, black, and red lines at the bottom of each plot are the fractions of the solid, intermediate, and liquid clusters present at each temperature.

plied by scaling factors. The simulation is fit to the measured heat capacities using a least-squares procedure with seven adjustable parameters:  $\Delta H_1$ ,  $T_1$ ,  $\Delta H_2$ ,  $T_2$ ,  $S_S$ ,  $S_I$ , and  $S_L$ , where the final three are the scale factors.

The unfilled circles in Fig. 4 show the result of this fit with the same values for  $\Delta T$  as used in the experiments ( $\Delta T=25$  K close to the peaks and 50 K away from the peaks). The fits to the experimental data for both peaks are very good. The solid blue line going through the data shows simulations with  $\Delta T=5$  K. The heat capacities calculated with  $\Delta T=5$  K go through the points, indicating that the values of  $\Delta T$  used in the experiments are small enough that the peaks are not significantly broadened. The green, black, and red lines beneath each heat capacity plot show the fraction of solid, intermediate, and liquid present at each temperature.

Table I shows a summary of the transition temperatures and enthalpy changes deduced from the fits of the three-state model to the measurements for  $\text{Al}_{84}^+$  to  $\text{Al}_{89}^+$ . For  $\text{Al}_{84}^+$ ,  $\text{Al}_{88}^+$ , and  $\text{Al}_{89}^+$  the enthalpy change for the lower temperature transition is smaller than for the higher temperature one, while for  $\text{Al}_{85}^+$ ,  $\text{Al}_{86}^+$ , and  $\text{Al}_{87}^+$  the enthalpy change for the lower temperature transition is the larger.

TABLE I. Transition temperatures and enthalpy changes determined from the fits of the three-state model (see text) to the experimental results for  $\text{Al}_{84}^+$  to  $\text{Al}_{89}^+$ .

Cluster	Low temperature transition		High temperature transition	
	Temperature (K)	Enthalpy (kJ/mol)	Temperature (K)	Enthalpy (kJ/mol)
$\text{Al}_{84}^+$	467	100	584	109
$\text{Al}_{85}^+$	471	112	594	91
$\text{Al}_{86}^+$	513	143	585	75
$\text{Al}_{87}^+$	516	113	585	78
$\text{Al}_{88}^+$	501	110	617	148
$\text{Al}_{89}^+$	514	102	626	154

#### IV. EXPERIMENTAL RESULTS FOR ANNEALED CLUSTERS

In the annealing experiments the clusters are heated to a known temperature before their temperature is set for the heat capacity measurements. Annealing is a useful tool to investigate the origin of the dips and peaks observed in the heat capacities.<sup>31,40</sup> Annealing studies were performed for  $\text{Al}_{84}^+$  to  $\text{Al}_{89}^+$ ,  $\text{Al}_{115}^+$  to  $\text{Al}_{117}^+$ , and  $\text{Al}_{126}^+$  to  $\text{Al}_{128}^+$ . The results for  $\text{Al}_{115}^+$  to  $\text{Al}_{117}^+$  have been reported elsewhere.<sup>31</sup> Briefly, the low temperature peak disappears when these clusters are annealed to 523 K (a temperature between the two peaks) or to 773 K (well above both peaks). The high temperature peak persists unchanged for both annealing temperatures.

$\text{Al}_{126}^+$  to  $\text{Al}_{128}^+$  have dips in their heat capacities at a lower temperature than the peak. This behavior could result from the clusters being generated in the source in a geometry that is not the lowest enthalpy one. When the cluster is heated it converts into the lower enthalpy geometry yielding a dip in the heat capacity. If this is the case, the dip should disappear if the clusters are annealed to above the temperature of the dip. Figure 3 shows heat capacities measured for  $\text{Al}_{128}^+$  in the region of the dip. The black points show the results for unannealed clusters. The red points show the results after annealing to a temperature of 523 K (which is between the dip and peak). The dip has disappeared. Similar results were obtained for  $\text{Al}_{126}^+$  and  $\text{Al}_{127}^+$ . Note that in Fig. 3, the measurements for the annealed clusters were performed with  $\Delta T=25$  K, while those for the unannealed clusters near the dip used  $\Delta T=50$  K, so there are more data points across the dip for the annealed cluster than for the unannealed. For all three clusters,  $\text{Al}_{126}^+$ ,  $\text{Al}_{127}^+$ , and  $\text{Al}_{128}^+$ , the dip disappears when they are annealed.

For  $\text{Al}_{84}^+$ ,  $\text{Al}_{85}^+$ ,  $\text{Al}_{88}^+$ , and  $\text{Al}_{89}^+$  there are bimodal peaks in the heat capacities for unannealed clusters. When annealed to 823 K (above both peaks), the peaks stay bimodal. Peaks for clusters with 86 and 87 atoms are broad, and remain broad when these clusters are annealed. Some examples are shown in Fig. 5. The peaks for the 84 and 89 atom clusters remain bimodal when they are annealed (red points in the figure), and the peak for the 87 atom cluster remains broad. From the plot shown in Fig. 5 it is evident that there is a broad dip in the heat capacities for  $\text{Al}_{87}^+$  just above 300 K which disappears (like that for  $\text{Al}_{126}^+$ ,  $\text{Al}_{127}^+$ ,

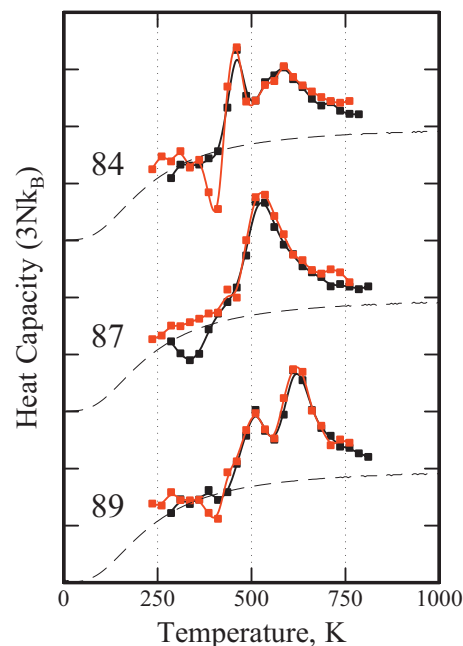


FIG. 5. Comparison of the heat capacities recorded for unannealed  $\text{Al}_{84}^+$ ,  $\text{Al}_{87}^+$ , and  $\text{Al}_{89}^+$  (filled black points and black line) to those recorded after annealing to 823 K (filled red points and red line). The black dashed lines are the heat capacities from the modified Debye model (Ref. 41).

and  $\text{Al}_{128}^+$ ) when the clusters are annealed. In the case of  $\text{Al}_{84}^+$  a dip emerges at around 400 K when the clusters are annealed.

#### V. DISCUSSION

##### A. The origin of the dips

A peak in the heat capacity indicates a transition to a higher enthalpy state as the temperature is raised. The transition is driven by entropy. Melting is one example of this behavior: the liquid state has a higher enthalpy, but it also has a higher entropy and so the liquid becomes thermodynamically preferred at some point as the temperature is raised. When the transition occurs the components may be in equilibrium, or the transition could occur under kinetic control with a superheated lower temperature phase.

A dip in the heat capacity indicates a transition to a lower enthalpy state as the temperature is raised. In this case, the lower enthalpy state is thermodynamically preferred, so for a dip to exist the system must be kinetically trapped in the higher enthalpy state. As the temperature is raised the rate constant for the transition to the low enthalpy state increases until the transition occurs on the timescale of the experiments.

All the dips can be attributed to one of two scenarios. In the first, the system is trapped in a high enthalpy state during cluster growth. For example, if the lowest energy geometry changes from icosahedral to fcc as the cluster grows it can become trapped in the icosahedral geometry if there is insufficient energy to overcome the activation barrier to convert into fcc. The clusters grow by sequential addition of atoms, and each addition brings an excess energy equal to the dissociation energy to the cluster. This extra energy raises the temperature of the cluster which is subsequently cooled by

collisions with the buffer gas. The cluster will be trapped if its temperature remains below that required for the structural transition to occur on the experimental timescale.

As noted above, the dips in the heat capacities for  $\text{Al}_{126}^+$ ,  $\text{Al}_{127}^+$ , and  $\text{Al}_{128}^+$  disappear when these clusters are annealed. This behavior is consistent with the scenario outlined above; the clusters are trapped in a metastable geometry during cluster growth and then convert into the lower enthalpy structure as the temperature is raised.

There are also dips for some clusters with 84–90 atoms. For unannealed clusters the most obvious example is the dip at around 350 K for  $\text{Al}_{87}^+$ . This dip also disappears when the clusters are annealed. In the case of  $\text{Al}_{84}^+$ , a dip *emerges* when the clusters are annealed. This is clearly inconsistent with the explanation outlined above.

In previous work, dips have also been observed for several aluminum clusters with around 60 atoms (56, 57, 58, 60, 61, and 62)<sup>16</sup> and around 80 atoms (80, 81, 82, and 83).<sup>30</sup> For some of these clusters the dips disappear when they are annealed, but for others the dip persists even when the clusters are annealed to well above their melting temperature. In one case,  $\text{Al}_{83}^+$ , the dip increases when the cluster is annealed. This behavior is presumably related to that reported here for  $\text{Al}_{84}^+$  where the dip appears when the cluster is annealed.

In an effort to explain our previous results for clusters with around 60 and 80 atoms, we developed a kinetic model of melting and freezing for a system with one liquidlike and two solidlike states with different melting temperatures.<sup>40</sup> Using this model we were able to explain our previous experimental results. The thermodynamically preferred solid always has the higher freezing temperature. However, the liquid can bypass freezing into the thermodynamically preferred solid (at high cooling rates) if the higher energy geometry has a larger freezing rate. An analogous type of behavior occurs in macroscopic objects, for example, glass formation, where freezing into a crystalline geometry is kinetically hindered. In the clusters, freezing into the high energy geometry can occur as they are cooling down after cluster growth or after leaving the annealing section. The dips then result from isomerization into the thermodynamically preferred solid in the temperature variable extension. This is the second of the two scenarios mentioned above.

The dip that emerges for  $\text{Al}_{84}^+$  when this cluster is annealed can be safely attributed to this second origin—freezing into a high energy geometry. The dip does not appear for  $\text{Al}_{84}^+$  until after the cluster is annealed because the energy provided during cluster growth is insufficient to melt the cluster. But when the cluster is melted in the annealing section and then quenched when it leaves, the cluster freezes into a high energy geometry.

Could this second process also be responsible for the dips observed for  $\text{Al}_{126}^+$ ,  $\text{Al}_{127}^+$ , and  $\text{Al}_{128}^+$ ? This can be safely ruled out because the energy provided during cluster growth is insufficient to melt the clusters. For aluminum clusters in this size regime the dissociation energies are around 3.2 eV.<sup>28</sup> Assuming a classical heat capacity, when this energy is added to a 127-atom cluster it raises the temperature by around 100 K. The cluster source is held at around 300 K and so the clusters should transiently reach

around 400 K after the addition of one atom. It should take only around 1  $\mu\text{s}$  to remove the excess energy by collisions with the buffer gas.<sup>52</sup> According to the heat capacity plots shown in Fig. 1 the melting temperatures for  $\text{Al}_{126}^+$ ,  $\text{Al}_{127}^+$ , and  $\text{Al}_{128}^+$  are at around 650 K. It is unlikely that the clusters reach this temperature in the final stages of cluster growth. Instead, it seems much more likely that the dips for these clusters are caused by structural transitions which result because cluster growth does not lead to the lowest energy structure.

## B. The origin of the multiple peaks

Broad or bimodal peaks are observed in the heat capacities for aluminum clusters with 84 to 89 atoms. Two well-resolved peaks are observed for  $\text{Al}_{115}^+$ ,  $\text{Al}_{116}^+$ , and  $\text{Al}_{117}^+$ . We discussed the results for  $\text{Al}_{115}^+$ ,  $\text{Al}_{116}^+$ , and  $\text{Al}_{117}^+$  elsewhere.<sup>31</sup> On the basis of annealing studies the low temperature peaks were attributed to structural transitions from a low enthalpy, low entropy solid to a high enthalpy, high entropy solid, and the high temperature peak was attributed to a melting transition.

Altogether there are three possible explanations for a second (lower temperature) peak in the heat capacity: (1) a structural transition to a higher enthalpy state as discussed above, (2) partial melting of the cluster, and (3) two structures that melt at different temperatures. The third explanation can be ruled out on the basis of the annealing results. Annealing the 84–89 atom clusters has a negligible effect on the peaks in the heat capacity (see Fig. 5). If the two peaks in the heat capacity are due to isomers that melt at different temperatures then when the first isomer melts it has the opportunity to refreeze into the higher-melting temperature isomer. If it does refreeze this process becomes a solid to solid transition. For it not to refreeze, the freezing rate into the higher melting temperature isomer must be slow on the experimental time scale. If this was the case, the cluster would not refreeze into the high-melting temperature isomer when it is annealed. For the 84–89 atom clusters both peaks are recovered after annealing, so this explanation can be ruled out.

The second explanation listed above is partial melting of the cluster, where some part of the cluster melts before the rest. This could, for example, be the surface, the core, or a collection of weakly bound atoms within the cluster. Surface premelting has been observed in many simulations of cluster melting.<sup>53–58</sup> The signature of this behavior is a second peak, or a shoulder, in the heat capacity at a lower temperature than the main melting transition.

There are also plenty of examples from simulations for the first explanation given above—a structural transition to a higher enthalpy state. Structural transitions have been found to precede melting in a number of simulations of cluster melting,<sup>59–62</sup> including Lennard-Jones clusters.<sup>63–69</sup> It may not be possible to distinguish between partial melting and structural transitions on the basis of the annealing results. In both cases, annealing may not alter the peaks in the heat capacity. In the case of partial melting, annealing should not cause any change in the peaks. In the case of a structural

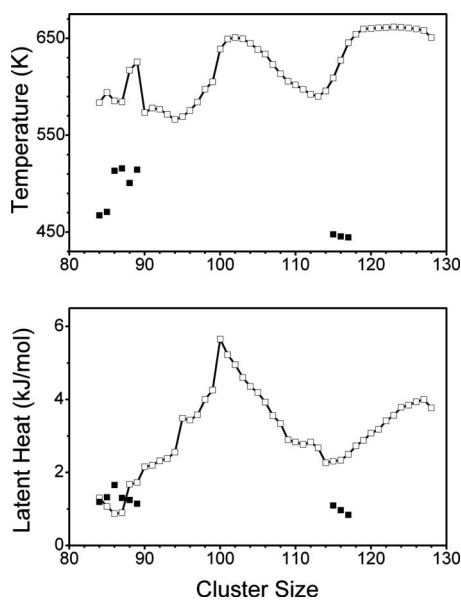


FIG. 6. Plot of the transition temperatures (top panel) and enthalpy changes (bottom panel) determined from the fits of the two-state and three-state models (see text) to the measured heat capacities for aluminum cluster cations with 84 to 128 atoms. The unfilled points show the temperatures and latent heats for the melting transition. The filled points show the temperatures and enthalpy changes for the lower temperature transition when it is observed.

transition, annealing will not cause any change if the structural transition occurs under equilibrium. For  $\text{Al}_{115}^+$ ,  $\text{Al}_{116}^+$ , and  $\text{Al}_{117}^+$  the low temperature peak disappears when the clusters are annealed, and we attributed the low temperature peak to a structural transition involving a superheated solid where the reverse process does not occur on our experimental timescale.<sup>31</sup> For  $\text{Al}_{84}^+$  to  $\text{Al}_{89}^+$  annealing does not make a significant difference to the peaks and so we cannot distinguish between a structural transition or partial melting.

### C. The fits, melting temperatures, and latent heats

Most of the clusters studied here show a single peak in the heat capacity that can be well fit by the two-state model. In particular, the width of the transition is reproduced. Within the framework of the model, the width is determined by an equilibrium between solid and liquid clusters. The temperature range over which the solid and liquid coexist is determined by the latent heat and the transition temperature. As the latent heat increases, the solid and liquid coexist over a narrower temperature range, and the transition becomes sharper. The good agreement between the experimental results and the predictions of the model confirms that the melting transition involves a dynamic phase coexistence.

Figure 6 shows a plot of the transition temperatures and enthalpy changes for aluminum cluster cations with 84 to 128 atoms, determined from the fits with the two- and three-state models described above. The open points show the melting temperatures and latent heats for the melting transitions while the filled points show the temperatures and enthalpies for the lower temperature transitions when they are

observed. Both the melting temperatures and latent heats are significantly smaller than the bulk values (933.5 K and 10.7 kJ/mol).

The melting temperatures for clusters in the size range examined here do not show the large size-dependent fluctuations observed for smaller aluminum clusters,<sup>10,30,32</sup> instead they show relatively smooth variations with size. The melting temperatures show a local maximum at  $\text{Al}_{88}^+$  and  $\text{Al}_{89}^+$ , and then there are broad steps in the melting temperature at around  $\text{Al}_{100}^+$  and  $\text{Al}_{117}^+$ . The melting temperatures vary over a range of around 100 K. Much larger changes have been observed for smaller cluster sizes.<sup>10,30,32</sup> In previous work we have shown that both geometry and electronic shell closings influence the melting temperatures.<sup>29</sup> Abrupt changes in melting temperatures are correlated with changes in the geometry of the lowest energy structure. There are substantial maxima in the melting temperatures around the spherical electronic shell closings with 138 (near  $\text{Al}_{46}^+$ ) and 198 (near  $\text{Al}_{66}^+$ ) valence electrons.<sup>70</sup> As noted in the Introduction, it is thought that these maxima result because the clusters around the spherical shell closings adopt near-spherical geometries that are disordered. Since  $T_m = \Delta H_m / \Delta S_m$ , the diminished entropy change on melting for the disordered structures causes an increase in the melting temperature (assuming that the enthalpy change is not impacted by the same amount). The next spherical electronic shell closing occurs at 274 valence electrons (near  $\text{Al}_{92}^+$ ). There is no substantial increase in the melting temperatures for clusters around  $\text{Al}_{92}^+$ , suggesting that the influence of the electronic shell closings on the melting temperatures diminishes as the cluster size increases.

We have shown elsewhere that the latent heats are correlated with the cohesive energies of the clusters.<sup>28</sup> The relationship between the dissociation energies and the latent heats is then<sup>28</sup>

$$D_S(n) \approx D_L(n) + L(n) - L(n-1), \quad (8)$$

where  $D_S(n)$  and  $D_L(n)$  are the dissociation energies (the energy required to remove one atom from the cluster) for the solid and liquid  $n$ -atom cluster, respectively. The liquidlike cluster does not exist at 0 K. However,  $D_L(n)$  is still a meaningful quantity because its value can be deduced by extrapolation from higher temperatures.  $L(n)$  and  $L(n-1)$  in Eq. (8) are the latent heats for the  $n$ -atom and  $(n-1)$ -atom cluster, respectively.  $D_L(n)$  is expected to change smoothly with cluster size, and so local fluctuations in the dissociation energies result mainly from differences between  $L(n)$  and  $L(n-1)$ . The quantity  $L(n) - L(n-1)$  provides a measure of the relative dissociation energy of the clusters. A plot of this quantity against cluster size is shown in Fig. 7. There are significant maxima in the relative dissociation energies at 88, 95, and 100 atoms. The origin of these features is not clear. There is no maximum at  $\text{Al}_{92}^+$ , near the spherical electronic shell closing with 274 valence electrons. So the observed maxima may be structure related: there may be a structural shell closing at  $\text{Al}_{100}^+$ . However, 300 valence electrons also corresponds to an electronic shell closing, so perhaps the special behavior of  $\text{Al}_{100}^+$  results from a combination of favorable structural and electronic effects.

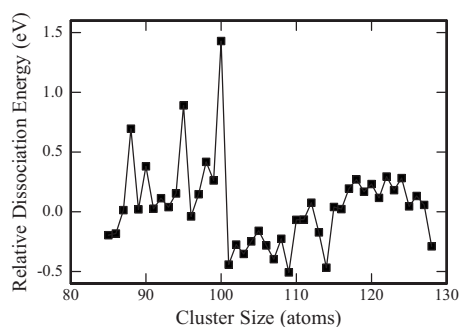


FIG. 7. Plot of the relative dissociation energies against cluster size. The relative dissociation energies were obtained from the latent heats using the approach described in the text.

Multiple peaks or bimodal peaks occur in the heat capacities when the latent heats (and hence also the cohesive energies) are small (see Fig. 6). This may reflect the structures that are present. Perhaps there is only one dominant stable structure present when the cohesive energies are large, but several structures compete when the cohesive energies are small. There may be a change in the basic structure at the minima in the latent heats (and cohesive energies). For example, if the clusters have a particular structure below the minimum and with increasing size, this structure becomes less favorable. Then a structural change will occur if a competing structure emerges at the minimum and becomes more favorable with increasing cluster size. The minimum in the latent heats (and cohesive energies) at around 116 atoms (see Fig. 6) is correlated with a sharp increase in the melting temperatures which may be another signature of a geometry change. On the other hand, the sharp increase in the melting temperatures at around 99 atoms is correlated with a peak in the latent heats (and cohesive energies).

## VI. CONCLUSIONS

There are peaks in the heat capacities for all cationic aluminum clusters with 84–128 atoms which are assigned to first-order melting transitions. In addition to the melting transitions, clusters with 84–89 atoms and 115–117 atoms have another peak. In the case of the 115–117 atom clusters, the low temperature peak is assigned to structural transition, for clusters with 84–89 atoms the additional peak may be due to partial melting or a structural transition. Clusters with 126–128 atoms have a dip in the heat capacity assigned to an irreversible structural transition to a lower enthalpy structure. The heat capacities are well fit by two-state or three-state models which assume dynamic phase coexistence. The abrupt changes in the melting temperatures and latent heats that were observed for smaller clusters are moderated in this larger size regime. However, there are still a number of prominent features, including, for example, a substantial maximum in the latent heats and hence the cohesive energy at  $\text{Al}_{100}^+$ . The enhanced stability of  $\text{Al}_{100}^+$  may result from a confluence of both structural and electronic factors.

## ACKNOWLEDGMENTS

We gratefully acknowledge the support of the National Science Foundation.

- <sup>1</sup>R. Ferrando, J. Jellinek, and R. L. Johnston, *Chem. Rev. (Washington, D.C.)* **108**, 845 (2008).
- <sup>2</sup>A. A. Shvartsburg and M. F. Jarrold, *Phys. Rev. A* **60**, 1235 (1999).
- <sup>3</sup>A. Aguado and J. M. López, *J. Chem. Phys.* **130**, 064704 (2009).
- <sup>4</sup>A. Lechtken, C. Neiss, M. M. Kappes, and D. Schooss, *Phys. Chem. Chem. Phys.* **11**, 4344 (2009).
- <sup>5</sup>E. C. Honea, A. Ogura, D. R. Peale, C. Felix, C. A. Murray, K. Raghavachari, W. O. Sprenger, M. F. Jarrold, and W. L. Brown, *J. Chem. Phys.* **110**, 12161 (1999).
- <sup>6</sup>C. Bréchnignac, P. Cahuzac, J. Leygnier, and J. Weiner, *J. Chem. Phys.* **90**, 1492 (1989).
- <sup>7</sup>U. Ray, M. F. Jarrold, J. E. Bower, and J. S. Kraus, *J. Chem. Phys.* **91**, 2912 (1989).
- <sup>8</sup>D. A. Hales, L. Lian, and P. B. Armentrout, *Int. J. Mass Spectrom. Ion Process.* **102**, 269 (1990).
- <sup>9</sup>M. Schmidt, R. Kusche, B. von Issendorff, and H. Haberland, *Nature (London)* **393**, 238 (1998).
- <sup>10</sup>C. M. Neal, A. K. Starace, and M. F. Jarrold, *Phys. Rev. B* **76**, 054113 (2007).
- <sup>11</sup>C. Hock, C. Bartels, S. Straßburg, M. Schmidt, H. Haberland, B. von Issendorff, and A. Aguado, *Phys. Rev. Lett.* **102**, 043401 (2009).
- <sup>12</sup>S. M. Ghazi, S. Zorriasatein, and D. G. Kanhere, *J. Phys. Chem. A* **113**, 2659 (2009).
- <sup>13</sup>G. A. Breaux, B. Cao, and M. F. Jarrold, *J. Phys. Chem. B* **109**, 16575 (2005).
- <sup>14</sup>P. Pawlow, *Z. Phys. Chem.* **65**, 1 (1909).
- <sup>15</sup>M. Schmidt, R. Kusche, W. Kronmüller, B. von Issendorff, and H. Haberland, *Phys. Rev. Lett.* **79**, 99 (1997).
- <sup>16</sup>G. A. Breaux, C. M. Neal, B. Cao, and M. F. Jarrold, *Phys. Rev. Lett.* **94**, 173401 (2005).
- <sup>17</sup>P. Blaise and S. A. Blundell, *Phys. Rev. B* **63**, 235409 (2001).
- <sup>18</sup>K. Manninen, A. Rytönen, and M. Manninen, *Eur. Phys. J. D* **29**, 39 (2004).
- <sup>19</sup>S. Chacko, K. Joshi, and D. G. Kanhere, *Phys. Rev. Lett.* **92**, 135506 (2004).
- <sup>20</sup>H. Haberland, T. Hippler, J. Donges, O. Kostko, M. Schmidt, and B. V. Issendorff, *Phys. Rev. Lett.* **94**, 035701 (2005).
- <sup>21</sup>A. Aguado and J. M. López, *Phys. Rev. Lett.* **94**, 233401 (2005).
- <sup>22</sup>A. Aguado, *J. Phys. Chem. B* **109**, 13043 (2005).
- <sup>23</sup>A. Aguado and J. M. López, *Phys. Rev. B* **74**, 115403 (2006).
- <sup>24</sup>K. Joshi, S. Krishnamurty, and D. G. Kanhere, *Phys. Rev. Lett.* **96**, 135703 (2006).
- <sup>25</sup>E. G. Noya, J. P. K. Doye, and F. Calvo, *Phys. Rev. B* **73**, 125407 (2006).
- <sup>26</sup>E. G. Noya, J. P. K. Doye, D. J. Wales, and A. Aguado, *Eur. Phys. J. D* **43**, 57 (2007).
- <sup>27</sup>C. M. Neal, A. K. Starace, M. F. Jarrold, K. Joshi, S. Krishnamurty, and D. G. Kanhere, *J. Phys. Chem. C* **111**, 17788 (2007).
- <sup>28</sup>A. K. Starace, C. M. Neal, B. Cao, M. F. Jarrold, A. Aguado, and J. M. López, *J. Chem. Phys.* **129**, 144702 (2008).
- <sup>29</sup>A. K. Starace, C. M. Neal, B. Cao, M. F. Jarrold, A. Aguado, and J. M. López, *J. Chem. Phys.* **131**, 044307 (2009).
- <sup>30</sup>C. M. Neal, A. K. Starace, and M. F. Jarrold, *J. Am. Soc. Mass Spectrom.* **18**, 74 (2007).
- <sup>31</sup>B. Cao, A. K. Starace, O. H. Judd, I. Bhattacharyya, and M. F. Jarrold, *J. Chem. Phys.* **131**, 124305 (2009).
- <sup>32</sup>G. A. Breaux, R. C. Benirschke, T. Sugai, B. S. Kinnear, and M. F. Jarrold, *Phys. Rev. Lett.* **91**, 215508 (2003).
- <sup>33</sup>G. A. Breaux, D. A. Hillman, C. M. Neal, R. C. Benirschke, and M. F. Jarrold, *J. Am. Chem. Soc.* **126**, 8628 (2004).
- <sup>34</sup>G. A. Breaux, C. M. Neal, B. Cao, and M. F. Jarrold, *Phys. Rev. B* **71**, 073410 (2005).
- <sup>35</sup>B. Cao, A. K. Starace, C. M. Neal, and M. F. Jarrold, *J. Chem. Phys.* **129**, 124709 (2008).
- <sup>36</sup>C. M. Neal, A. K. Starace, and M. F. Jarrold, *J. Phys. Chem. A* **111**, 8056 (2007).
- <sup>37</sup>F. Chiro, P. Feiden, S. Zamith, P. Labastie, and J. M. L'Hermite, *J. Chem. Phys.* **129**, 164514 (2008).
- <sup>38</sup>M. F. Jarrold and E. C. Honea, *J. Phys. Chem.* **95**, 9181 (1991).

- <sup>39</sup>C. M. Neal, G. A. Breaux, B. Cao, A. K. Starace, and M. F. Jarrold, *Rev. Sci. Instrum.* **78**, 075108 (2007).
- <sup>40</sup>M. F. Jarrold, B. Cao, A. K. Starace, and C. M. Neal, *J. Chem. Phys.* **129**, 014503 (2008).
- <sup>41</sup>J. Bohr, *Int. J. Quantum Chem.* **84**, 249 (2001).
- <sup>42</sup>D. Poland, *J. Chem. Phys.* **126**, 054507 (2007).
- <sup>43</sup>C. L. Briant and J. J. Burton, *J. Chem. Phys.* **63**, 2045 (1975).
- <sup>44</sup>R. S. Berry, J. Jellinek, and G. Natanson, *Phys. Rev. A* **30**, 919 (1984).
- <sup>45</sup>T. L. Beck, J. Jellinek, and R. S. Berry, *J. Chem. Phys.* **87**, 545 (1987).
- <sup>46</sup>H. Reiss, P. Mirabel, and R. L. Whetten, *J. Phys. Chem.* **92**, 7241 (1988).
- <sup>47</sup>P. Labastie and R. L. Whetten, *Phys. Rev. Lett.* **65**, 1567 (1990).
- <sup>48</sup>H.-P. Cheng, X. Li, R. L. Whetten, and R. S. Berry, *Phys. Rev. A* **46**, 791 (1992).
- <sup>49</sup>J. P. Rose and R. S. Berry, *J. Chem. Phys.* **98**, 3246 (1993).
- <sup>50</sup>B. Vekhter and R. S. Berry, *J. Chem. Phys.* **106**, 6456 (1997).
- <sup>51</sup>B. Cao, A. K. Starace, O. H. Judd, and M. F. Jarrold, *J. Chem. Phys.* **130**, 204303 (2009).
- <sup>52</sup>Assuming that each collision equilibrates only one vibrational degree of freedom in the cluster.
- <sup>53</sup>A. Aguado, J. M. Lopez, J. A. Alonso, and M. J. Stott, *J. Chem. Phys.* **111**, 6026 (1999).
- <sup>54</sup>F. Calvo and F. Spiegelmann, *J. Chem. Phys.* **112**, 2888 (2000).
- <sup>55</sup>Y. J. Lee, E.-K. Lee, and S. Kim, *Phys. Rev. Lett.* **86**, 999 (2001).
- <sup>56</sup>A. Aguado, L. M. Molina, J. M. Loez, and J. A. Alonso, *Eur. Phys. J. D* **15**, 221 (2001).
- <sup>57</sup>K. Joshi, D. G. Kanhere, and S. A. Blundell, *Phys. Rev. B* **67**, 235413 (2003).
- <sup>58</sup>F. Calvo and F. Spiegelmann, *J. Chem. Phys.* **120**, 9684 (2004).
- <sup>59</sup>C. L. Cleveland, W. D. Luedtke, and U. Landman, *Phys. Rev. Lett.* **81**, 2036 (1998).
- <sup>60</sup>D. Schebarchov and S. C. Hendy, *Phys. Rev. Lett.* **95**, 116101 (2005).
- <sup>61</sup>Z. Zhang, W. Hu, and S. Xiao, *Phys. Rev. B* **73**, 125443 (2006).
- <sup>62</sup>D. Schebarchov and S. C. Hendy, *Phys. Rev. B* **73**, 121402R (2006).
- <sup>63</sup>J. P. K. Doye and D. J. Wales, *Phys. Rev. Lett.* **80**, 1357 (1998).
- <sup>64</sup>J. P. K. Doye and F. Calvo, *J. Chem. Phys.* **116**, 8307 (2002).
- <sup>65</sup>V. A. Mandelshtam, P. A. Frantsuzov, and F. Calvo, *J. Phys. Chem. A* **110**, 5326 (2006).
- <sup>66</sup>E. G. Noya and J. P. K. Doye, *J. Chem. Phys.* **124**, 104503 (2006).
- <sup>67</sup>V. A. Mandelshtam and P. A. Frantsuzov, *J. Chem. Phys.* **124**, 204511 (2006).
- <sup>68</sup>V. A. Sharapov and V. A. Mandelshtam, *J. Phys. Chem. A* **111**, 10284 (2007).
- <sup>69</sup>L. Zhan, J. Z. Y. Chen, and W. K. Liu, *J. Chem. Phys.* **127**, 141101 (2007).
- <sup>70</sup>Note that the aluminum cluster cations do not have the precise number of electrons required to match the electronic shell closings:  $\text{Al}_{46}^+$  has 137 valence electrons (shell closing at 138),  $\text{Al}_{66}^+$  has 197 (shell closing at 198), and  $\text{Al}_{92}^+$  has 275 (shell closing at 274).